Molecular Imaging
Volume 15 : 1-11
© The Author(s) 2016
Reprints and permission:
sagepub.com/journalsPermissions.nav
DOI: 10.1177/1536012116644881
mix.sagepub.com
SAGE

Tryptophan PET Imaging of the Kynurenine Pathway in Patient-Derived Xenograft Models of Glioblastoma

Anthony R. Guastella, BS[1,2], Sharon K. Michelhaugh, PhD[1], Neil V. Klinger, MS[1], William J. Kupsky, MD[3,4], Lisa A. Polin, PhD[2,4], Otto Muzik, PhD[5,6,7], Csaba Juhász, MD, PhD[4,5,7,8], and Sandeep Mittal, MD, FRCSC, FACS[1,2,4]

Abstract

Increasing evidence demonstrates the immunosuppressive kynurenine pathway's (KP) role in the pathophysiology of human gliomas. To study the KP in vivo, we used the noninvasive molecular imaging tracer α-[^{11}C]-methyl-L-tryptophan (AMT). The AMT-positron emission tomography (PET) has shown high uptake in high-grade gliomas and predicted survival in patients with recurrent glioblastoma (GBM). We generated patient-derived xenograft (PDX) models from dissociated cells, or tumor fragments, from 5 patients with GBM. Mice bearing subcutaneous tumors were imaged with AMT-PET, and tumors were analyzed to detect the KP enzymes indoleamine 2,3-dioxygenase (IDO) 1, IDO2, tryptophan 2,3-dioxygenase, kynureninase, and kynurenine 3-monooxygenase. Overall, PET imaging showed robust tumoral AMT uptake in PDX mice with prolonged tracer accumulation over 60 minutes, consistent with AMT trapping seen in humans. Immunostained tumor tissues demonstrated positive detection of multiple KP enzymes. Furthermore, intracranial implantation of GBM cells was performed with imaging at both 9 and 14 days postimplant, with a marked increase in AMT uptake at 14 days and a corresponding high level of tissue immunostaining for KP enzymes. These results indicate that our PDX mouse models recapitulate human GBM, including aberrant tryptophan metabolism, and offer an in vivo system for development of targeted therapeutics for patients with GBM.

Keywords

indoleamine 2,3-dioxygenase, tryptophan 2,3-dioxygenase, α-[^{11}C]-methyl-L-tryptophan, patient-derived xenograft, orthotopic mouse model

Introduction

Glioblastoma (GBM) is a World Health Organization (WHO) grade IV glioma and is the most common primary malignancy of the central nervous system (CNS), with an annual age-adjusted incidence rate of 3.19 per 100 000.[1] Approximately 10 200 new cases with GBM are predicted for 2015 in the United States alone.[1] Despite the ~160 US Food and Drug Administration–approved drugs for cancer treatment, only 3 are approved for treating GBMs: temozolomide (TMZ), biodegradable carmustine wafers, and bevacizumab.[2] Multimodal standard-of-care treatment for GBM consists of aggressive surgical resection, concurrent radiotherapy, and chemotherapy with TMZ after surgery, followed by 6 to 12 months of adjuvant TMZ therapy. Even with this aggressive treatment regimen, median survival of patients with GBM remains dismal at 12 months, with the 5-year survival rate less than 5%.[3,4] With this bleak outlook for

[1] Department of Neurosurgery, Wayne State University, Detroit, MI, USA
[2] Department of Oncology, Wayne State University, Detroit, MI, USA
[3] Department of Pathology, Wayne State University, Detroit, MI, USA
[4] Karmanos Cancer Institute, Detroit, MI, USA
[5] Department of Pediatrics, Wayne State University, Detroit, MI, USA
[6] Department of Radiology, Wayne State University, Detroit, MI, USA
[7] PET Center and Translational Imaging Laboratory, Children's Hospital of Michigan, Detroit, MI, USA
[8] Department of Neurology, Wayne State University, Detroit, MI, USA

Submitted: 02/09/2015. Revised: 04/03/2016. Accepted: 18/03/2016.

Corresponding Author:
Sandeep Mittal, Department of Neurosurgery, Wayne State University, 4160 John R Street, Suite 930, Detroit, MI, 48201, USA.
Email: smittal@med.wayne.edu

patients with GBM, it is paramount to develop novel therapies with greater efficacy for GBM tumor cells.

Tryptophan (TRP) is an essential amino acid necessary for protein synthesis. However, only 1% of dietary TRP is incorporated into proteins. The bulk of TRP is therefore available for metabolism via 4 pathways to produce physiologically important metabolites including serotonin, melatonin, tryptamine, and kynurenine (KYN). Over 95% of TRP is metabolized to KYN via the kynurenine pathway (KP; Figure 1).[5] Through local TRP depletion and the production of the toxic metabolites, the KP fosters an immunosuppressive tumor microenvironment.[6,7] Three distinct enzymes are able to complete the initial and rate-limiting step of the metabolism of TRP to *N*-formylkynurenine (NFK): indoleamine 2,3-dioxygenase 1 (IDO1), indoleamine 2,3-dioxygenase 2 (IDO2), and tryptophan 2,3-dioxygenase 2 (TDO2). Formamidase rapidly converts NFK to KYN, which is further transformed to toxic metabolites by either kynurenine 3 monooxygenase (KMO) or kynureninase (KYNU). Recent studies have identified a potentially prominent role of the KP in the pathophysiology of gliomas.[8-10] Although both IDO1 and TDO2 have been identified in GBMs,[11-13] more recent studies suggest that TDO2 is the primary enzyme for TRP catabolism in GBM[9,10] and that the KYN produced is an endogenous ligand for the aryl hydrocarbon receptor (AHR).[9] The AHR (previously known as the dioxin receptor) is a transcription factor that, when activated, leads to enhanced survival and invasiveness of human GBM cells.[14] Inhibition of the overactivated KP in gliomas by enzyme inhibitors may represent a novel therapeutic approach to inhibit AHR activation and extend survival.[15] Therefore, because we utilize immunocompromised animals, we have a model system to study the intrinsic tumoral component of the KP-AHR axis.

To study TRP metabolism in vivo, the positron emission tomography (PET) tracer α-[^{11}C]-methyl-L-tryptophan (AMT), an analog of TRP originally designed to detect serotonin synthesis,[16-18] has proven useful in neuro-oncological applications. The AMT-PET scans showed very high uptake in both low- and high-grade gliomas.[19-21] Subsequent studies defined AMT-PET's advantages over standard magnetic resonance imaging (MRI) and fludeoxyglucose-PET[17,19,22] and found that AMT-PET could predict survival in patients with GBM having recurrent disease.[23] Here, we report the first use of this tracer within animal models of patient-derived GBM. Patient-derived xenografts (PDXs) were generated with immunocompromised mice by subcutaneous (subQ) implantation of GBM cells or tumor fragments in the flank or by intracranial injection of GBM cells. All PDX models were imaged with AMT-PET prior to collection of tissue for assay of KP enzyme levels.

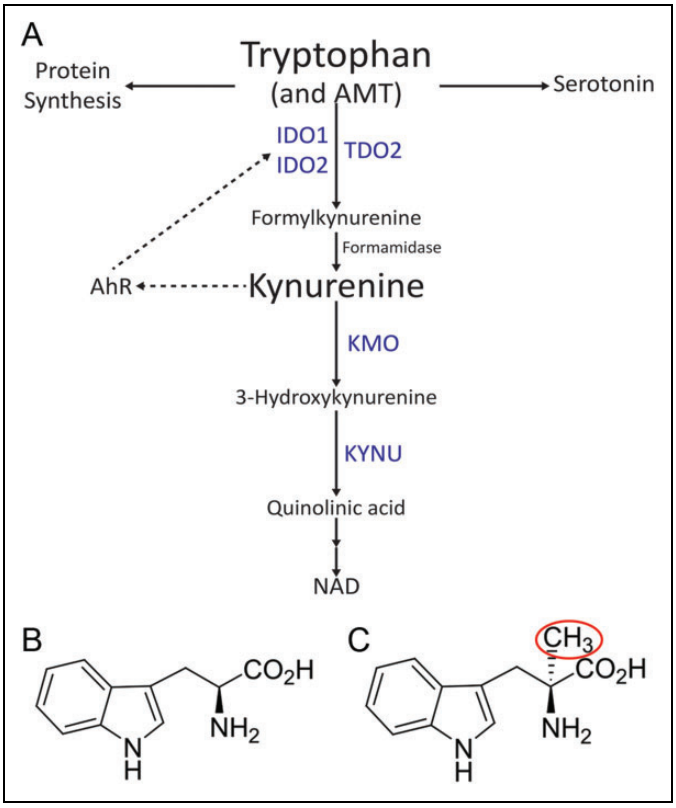

Figure 1. The kynurenine (KYN) pathway of tryptophan metabolism. (A) A simplified overview of the kynurenine pathway which metabolizes both tryptophan and α-[^{11}C]-methyl-L-tryptophan (AMT). Enzymes in blue represent those analyzed by immunohistochemistry. Dotted arrows represent a potential feedback pathway whereby KYN-activated aryl hydrocarbon receptor (AHR) can regulate indoleamine 2,3-dioxygenase (IDO) 1/2 expression. (B) Chemical structure of tryptophan. (C) Chemical structure of AMT. Red circle indicates the radioactive methyl group.

Materials and Methods

Patient-Derived Tumor Specimens

The Wayne State University Institutional Review Board approved the study, and written informed consent was obtained from all patients. Active tumor tissues (without any necrosis, defined by the neurosurgeon) were acquired immediately following microsurgical resection after adequate materials were reserved for histopathological diagnosis. Tumor samples were divided, and based upon the collected specimen size, were used for a combination of the following: (i) formalin fixation, (ii) fragment for mouse implantation, and/or (iii) dissociation into single cell suspension for in vitro culture. Characteristics of the patients are outlined in Table 1.

Generation of Mouse Xenograft GBM Tumors

The Wayne State University Institutional Animal Care and Use Committee approved all animal experiments. Female SCID NCr BALB/c background mice (Charles River, Wilmington, Massachusetts), 4 to 6 weeks old, were used for all experiments. Patient specimens were collected at time of resection, and fragments were cut into pieces weighing ~30 mg and implanted subcutaneously into the flank of mice and/or the tumor was dissociated into a single cell suspension following the manufacturer's protocol for the GentleMACS Dissociator (Miltenyi Biotec, San Diego, California) in conjunction with the Human Tumor Dissociation kit

Table 1. Patient Characteristics and Source for Mouse Model Generation.

Tumor ID	Patient Age, Years	Gender	Newly Diagnosed or Recurrent GBM	Previous Treatment	Source Used to Generate Xenograft Model
10-040	59	M	Newly diagnosed	None	Cultured cells
13-058	48	M	Recurrent	Standard-of-care chemoradiation	Uncultured cells
13-062	66	F	Newly diagnosed	None	Cultured cells
14-041	50	F	Newly diagnosed	None	Tumor fragments
14-066	62	M	Newly diagnosed	None	Tumor fragments

Abbreviation: F, female; GBM, glioblastoma; M, male.

(Miltenyi Biotec). Single cell suspensions (freshly dissociated or cultured in vitro) were mixed with an equal volume of Matrigel Basement Membrane Matrix (BD Biosciences, San Jose, California) prior to injection into the flank. Each subQ injection site was injected with 3×10^6 GBM cells. Tumor growth and animal health were monitored twice weekly.

Orthotopic Mouse Model

A single cell suspension of GBM cells was prepared from subQ xenograft tumor fragments derived from GBM specimen 10-040 following the GentleMACS procedure described earlier, and cells were suspended in Roswell Park Memorial Institute (RPMI) 1640 media (1.5×10^6 cells/10 μL). Stereotactic intracranial GBM cell implantation was performed with the Just For Mice Stereotaxic Instrument and the Nanomite Programmable Syringe Pump (Harvard Apparatus, Holliston, Massachusetts) as described previously.[24] Briefly, mice weighing between 18 and 20 g were anesthetized and the cranium exposed. A burr hole was drilled 1 mm anterior of bregma and 1 mm lateral from the midline. Needle insertion, injection 3 mm below the cortical surface, and needle withdrawal were performed over a 10-minute period. The burr hole was sealed with bone wax and the incision closed with 1 to 2 sutures. Postoperatively, mice were monitored for overall health for 10 days.

Patient MRI and AMT-PET Scans

Diagnostic MRI scan performed on a Philips Achieva TX 3.0 Tesla (Philips, Andover, Massachusetts) magnet with routine postgadolinium T1-weighted (T1-Gad), T2-weighted, and fluid-attenuated inversion recovery axial images acquired 1 week prior to the AMT-PET were used for the patients in this study. The AMT-PET was performed using a Siemens EXACT/HR whole-body PET (Seimens Medical Solutions USA, Inc, Malvern, Pennsylvania). The in-plane resolution of the PET image was 7.5 ± 0.4 mm at full-width half-maximum and 7.0 ± 0.5 mm at full-width half-maximum in the axial direction. The AMT tracer was synthesized using a high-yield procedure as outlined previously.[25] The procedure for AMT-PET scanning has previously been described in detail.[20] In short, after a 6-hour fast, a single dose of AMT (3.7 MBq/kg) was injected intravenously over 2 minutes. Twenty-five minutes after tracer injection, a dynamic PET scan of the brain was obtained in 5-minute frames for 35 minutes (7 images taken in total). Measured attenuation correction, scatter, and decay correction were applied to all PET images.

Mouse Xenograft AMT-PET and Computed Tomography Scans

The AMT tracer was synthesized following the same protocol used for human studies.[25] For each tumor model, the mouse with the greatest tumor burden was selected for PET/computed tomography (CT) imaging from each group of 2 to 3 mice. Mice were fasted for 4 hours then injected intravenously with a single dose of the AMT tracer, ranging from 400 to 800 μCi. Mice were then anesthetized using isoflurane and placed in a MicroPET R4 scanner (Concorde Microsystems Inc, Knoxville, Tennessee) with in-plane resolution of 1.76 mm at full-width half-maximum in center of field of view and linear resolution of less than 2.5 mm in all 3 dimensions. Scans were initiated 5 to 6 minutes postinjection and lasted 60 minutes, with data collected in 10-minute frames. Following the hour-long PET imaging, a CT scan was obtained using an Inveon single-photon emission computed tomography (SPECT)/CT small animal imager (Siemens Medical Solutions USA, Inc).

All mouse AMT-PET images were analyzed using AMIDE software (Amide's a Medical Image Data Examiner version 1.0.4).[26] The CT and PET images were coregistered, and regions of interest (ROIs) were drawn on the tumor mass as defined using the CT scan. Mean radioactivity data were collected from each 10-minute frame and converted into an AMT standardized uptake value (SUV). The SUV was calculated as the ratio of the mean score from the calculated ROI statistics, to the injected dose (in μCi) divided by the mouse body weight (in kg). In the case of mice bearing multiple tumors, the SUV from the tumor with highest uptake was used for calculations and subsequent tissue studies.

Immunohistochemistry of Primary Tumor Tissue and Xenograft Mouse Tumors

Tissue from the original patient tumors and the subsequent mouse tumors were fixed in formalin and paraffin embedded before sectioning and proceeding with immunostaining procedures using the anti-rabbit VECTASTAIN Elite ABC kit (Vector Labs, Burlingame, California) following the manufacturer's protocol. After rehydrating the tissue, a citrate-based antigen unmasking solution was used (H-3300; Vector Labs) as

directed. Unmasking solution was warmed in 55°C water for 40 minutes. Tissues were first placed in the warmed solution and then in a steamer for 20 minutes. Primary antibodies used targeted the following proteins: IDO1 (0.1 mg/mL; cat.#NBP1-87702; Novus Biologicals, Littleton, Colorado), IDO2 (0.5 mg/mL; cat.#OAAB08672; Aviva Systems Biology, San Diego, California), TDO2 (0.3 mg/mL; cat# NBP2-13424; Novus Biologicals), KYNU (0.05 mg/mL; cat.#NBP1-56545; Novus Biologicals), KMO (concentration not provided by manufacturer; cat.#10698-1-AP; Proteintech, Chicago, Illinois), AHR (0.73 mg/mL; cat.#ab153744; Abcam, Cambridge, Massachusetts), and L-type amino acid transporter 1 (LAT1; 0.5 mg/mL; cat.#ab85226; Abcam). All primary antibodies used are anti-human rabbit antibodies and were used at a dilution of 1:100, except IDO2, which was used at a 1:50 dilution. The peroxidase substrate was Vector ImmPACT DAB solution (cat.#SK-4105; Vector Labs). Sections were counterstained with hematoxylin and mounted with VectaMount (cat.#H-500; Vector Labs). Secondary antibody only (no primary antibody) staining was performed as controls. Stained sections for each enzyme were scored by 4 of the investigators as follows: 0 = no staining; 1 = mild staining; 2 = moderate staining; and 3 = strong staining in at least 3 representative fields of view for all tumor samples. Hematoxylin and eosin (H&E) staining was performed following a standard protocol.[27]

Statistical Analysis

All statistical analyses were performed using GraphPad Prism version 6.05 for Windows (GraphPad Software, La Jolla, California). Immunohistochemical (IHC) scores and tumoral SUVs were entered (for each 10-minute frame), and Pearson correlations and linear regression tests were performed. A P value of .05 or less was considered statistically significant.

Results

Validation of 13-058 GBM PDX

Patient 13-058 presented with a recurrent WHO grade IV GBM in the left temporal lobe, as seen in the T1-Gad MRI in Figure 2A. The AMT-PET imaging of the patient showed robust tumoral tracer uptake at 30 to 55 minutes postinjection (Figure 2B). Coregistered images of MRI and AMT-PET revealed that the AMT uptake extended beyond the contrast-enhancing mass (Figure 2C), as is commonly seen in GBMs.[28] The resected 13-058 patient tumor was dissociated into cells, which were then injected into the flank of mice subQ and resulted in subQ flank tumors (Figure 2D). In the corresponding 13-058 mouse model, the AMT tracer also showed pronounced uptake on PET imaging (Figure 2E and F). In order to assess the KP components in the patient and corresponding mouse model, tumor tissues were analyzed via IHC staining (Figure 3). Not surprisingly, we observed high immunostaining in both the 13-058 patient tumor and the corresponding mouse tumor for LAT1, the main transporter responsible for the tracer uptake from blood to tumor tissue. Staining for the rate-limiting enzymes showed that IDO1 levels were low, while IDO2 and TDO2 levels were high. The downstream enzymes KP, KMO, and KYNU displayed strong immunostaining in both the patient and the mouse. Overall, the immunostaining and AMT-PET imaging results indicated that the mouse model accurately recapitulated the patient tumor characteristics.

Development and Characterization of SubQ Flank GBM PDXs

Four additional subQ flank PDX models (10-040, 13-062, 14-041, and 14-066) were established using 2 methods: 10-040 and 13-062 were generated from implanted cells, while 14-041 and 14-066 were generated from implanted patient tumor fragments. Both methods proved effective, and all 4 formed tumors. The H&E staining was performed for each tumor. The 10-040 mouse tumor showed abnormal cell morphology, hyperchromatic nuclei, along with atypical mitotic figures (Figure 4A, inset). The 13-062 mouse tumor displayed very high cellular density and areas of microvascular proliferation (Figure 4B, inset). The 14-041 mouse tumor exhibited pleomorphic cells with numerous mitotic figures that were often atypical (Figure 4C, inset). The 14-066 mouse tumor displayed unusual cellular composition; although this tumor had abnormal mitotic figures as seen in other tumor tissues, it exhibited low tumor cell density, large depositions of fat as well as abundant stromal tissue (Figure 4D, inset). When tumors reached an adequate size to be visible on CT, $\sim$200 mg, mice were imaged with AMT-PET (Figure 4A-D). Tissue immunostaining of 10-040, 13-062, 14-041, and 14-066 (Figures 5 and 6) all showed strong signals for LAT1, while IDO1 immunostaining was low in all tissues. Although 10-040 showed high levels of immunostaining for IDO2, 14-041 only had moderate immunostaining, and 13-062 and 14-066 showed no immunostaining at all. All 10-040, 13-062, and 14-041 showed modest levels of immunostaining for TDO2. The 14-066 showed very low immunostaining for TDO2, limited to only a few cells within the tissue. The KMO immunostaining was moderate for all tumors, whereas KYNU was high for all tumors.

Orthotopic PDX of 10-040 GBM

A 10-040 subQ mouse tumor was dissociated into a single cell suspension and successfully developed the 10-040 intracranial PDX model. The AMT-PET imaging was used to measure the initial in vivo KP characteristics of the intracranial GBM on postoperative day (POD) #9, with a second PET scan performed on day #14 (Figure 7A). On POD #9, there was modest uptake of the AMT tracer, while on POD #14 there was robust tumoral uptake with a 50% increase in tracer uptake. Subsequent analysis of tumor tissue was performed via IHC staining (Figure 6). Tumor immunostaining showed high levels of LAT1. All 3 of the rate-limiting enzymes—IDO1, IDO2, and TDO2—showed strong immunostaining. The KMO immunostaining was moderate, while KYNU expression was very strong. The AHR, which is activated by various KP metabolites, displayed strong

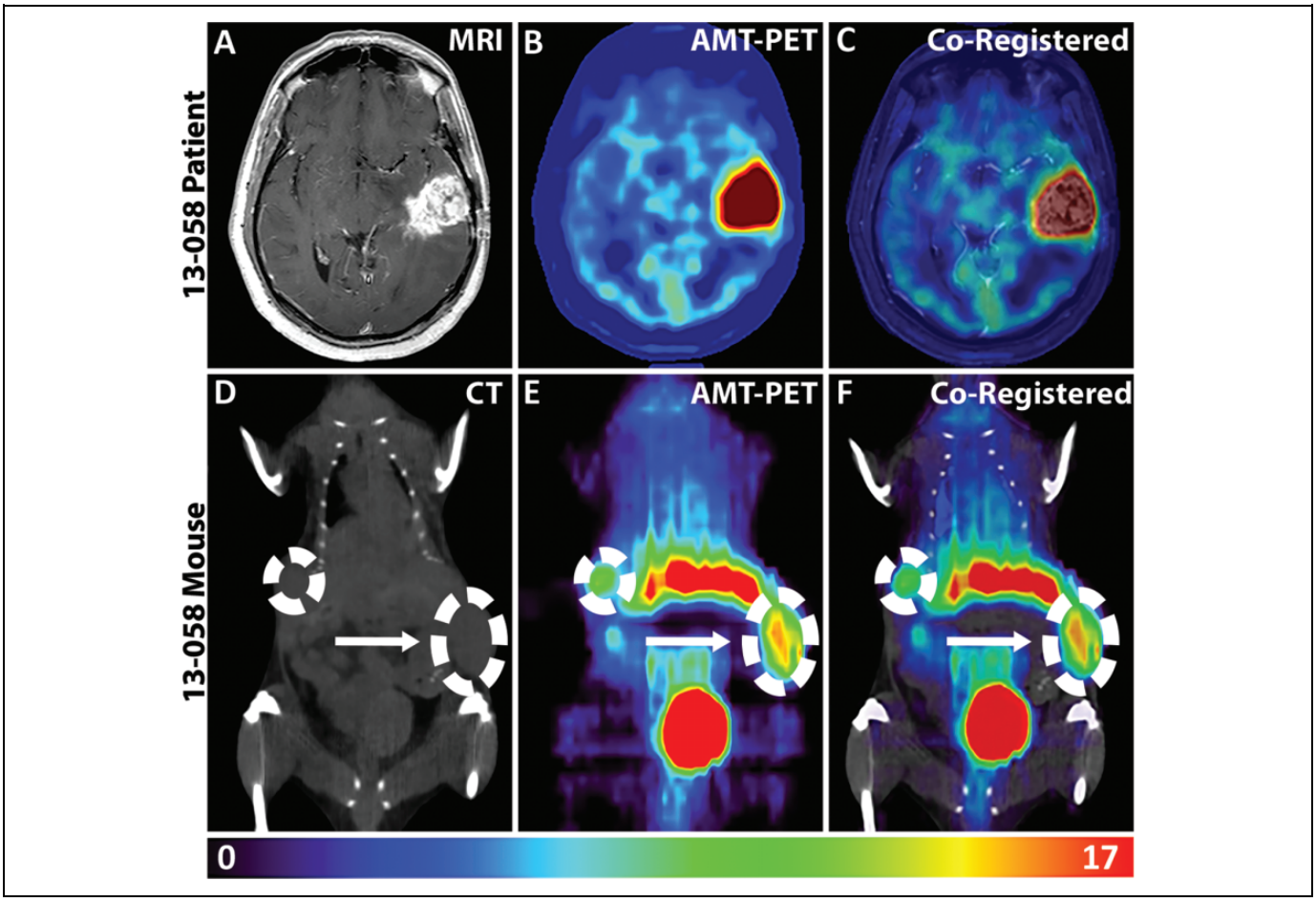

Figure 2. α-[^{11}C]-Methyl-L-tryptophan (AMT)-positron emission tomography (PET) imaging of patient with glioblastoma and corresponding patient-derived xenograft (PDX) model. AMT-PET imaging of the original patient and the accompanying xenograft model. A, Axial postcontrast T1-weighted magnetic resonance imaging (MRI) showing a recurrent left temporal glioblastoma. B, AMT-PET scan showed robust tracer uptake in the tumor (summed images 30-55 minutes postinjection). C, Coregistered patient AMT-PET and MRI scan. AMT uptake occurs beyond the area defined by the contrast-enhanced MRI. D, Mouse computed tomography (CT) scan identifies subcutaneous bilateral glioblastoma (GBM) tumors in the flank. E, Both subcutaneous tumors demonstrate marked AMT uptake (summed images 40-50 minutes postinjection). F, Coregistered CT and AMT-PET of PDX mouse model. Arrow indicates the larger tumor used for calculation of standardized uptake value (SUV) and subsequent tissue analyses. Colored scale bar at the bottom of the figure represents the range of SUVs for the mouse PET imaging.

immunostaining in the subQ model and very strong expression in the orthotopic intracranial model. Averaged immunostaining scores are shown in Figure 8A. The SUVs measured at the 10-minute frame on the PET scan showed a significant correlation with TDO2 IHC scores ($r = .83$, $P = .042$; Figure 8B). Furthermore, there was a significant correlation between the KYNU IHC scores and the SUVs at 30, 40, and 50 minutes (data not shown), and a highly significant correlation observed at 60 minutes ($r = .98$, $P = .0005$; Figure 8C).

Discussion

Glioblastomas represent the most common primary malignancy of the CNS with approximately 13 000 patients succumbing to the disease every year in the United States alone. Even with aggressive treatment, survival of patient with GBM is dreadfully low with a 5-year survival rate of less than 5%.[3,4] This underscores the urgency of developing novel therapies to incorporate into the standard of care. The KP (Figure 1A) offers researchers an innovative avenue to search for potential GBM therapies, as it is responsible for majority of the TRP catabolism in the CNS and has been found to be active within numerous human tumor types, including GBMs.[5,8,11,13] Furthermore, beyond simply depleting TRP, the enzymes involved in the pathway have been linked to tumoral immune resistance.[29] As such, enzymes of the KP are currently targets for development of new therapies, with a number of clinical trials evaluating the use of the IDO inhibitor indoximod (1-MT),[30-33] and the IDO1 inhibitor INCB024360 (epacadostat) for treatment of various extracranial cancers.[34-38] Clinical trials specifically for intracranial tumors with indoximod,[39] and the IDO2 inhibitor chloroquine,[40] are also underway.[41,42]

As pharmaceutics targeting the enzymes of the KP are further developed, noninvasive in vivo imaging using TRP

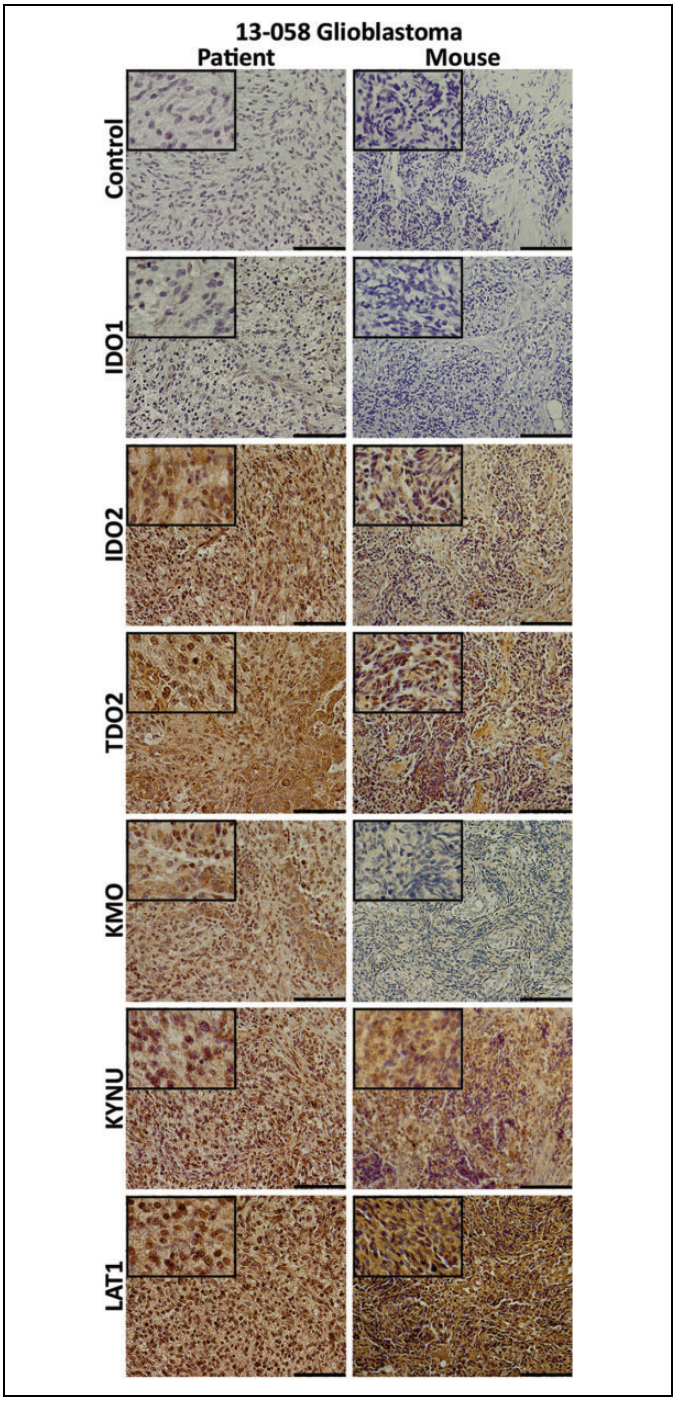

Figure 3. Immunostaining for kynurenine pathway's (KP) elements in patient and xenograft tumor tissues. Immunohistochemical staining for secondary antibody only control; the rate-limiting enzymes indoleamine 2,3-dioxygenase (IDO) 1, IDO2, and tryptophan 2,3-dioxygenase (TDO2); downstream enzymes kynureninase (KYNU) and kynurenine 3-monooxygenase (KMO); and L-type amino acid transporter 1 (LAT1), the membrane transporter that mediates the uptake of TRP and AMT. Left column: 13-058 patient tumor tissue and right column: mouse xenograft tumor tissue. Staining patterns are parallel between the 2 tumors with stronger signals found from IDO2 and TDO2 and the weakest signals found from IDO1 and KMO. The length of the scale bar is 100 μm. Insets: 4× greater magnification than the larger image.

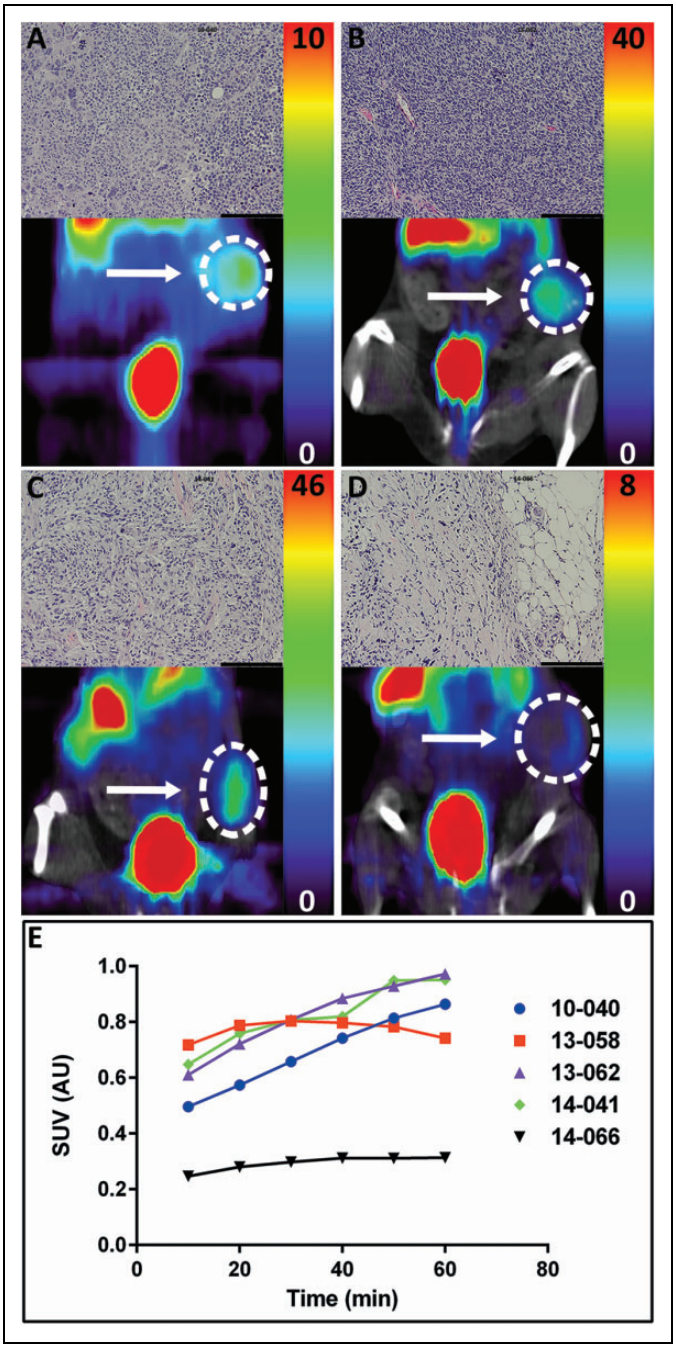

Figure 4. α-[^{11}C]-Methyl-L-tryptophan (AMT)-positron emission tomography (PET) imaging of patient-derived xenograft (PDX) glioblastoma (GBM) models. NCr SCID mice-bearing human GBM tumors, introduced either as a single cell suspension or as ~30 mg tumor fragments, were injected with AMT tracer. PET scans were performed for 60 minutes. Tumor models scanned were (A) 10-040 (PET scan only), (B) 13-062, (C) 14-041, and (D) 14-066. (B-D) PET coregistered with computed tomography (CT). Colored scale bars to the right of images indicate the range of standardized uptake values (SUVs) for each individual mouse. Insets: Corresponding hematoxylin and eosin (H&E) stains from each xenograft tumor. The length of the scale bar is 100 μm. (E) Plot of time versus the SUVs for AMT-PET scans of 5 different PDX GBM models. For 3 of the 5, peak AMT uptake was reached at the end of the scan period.

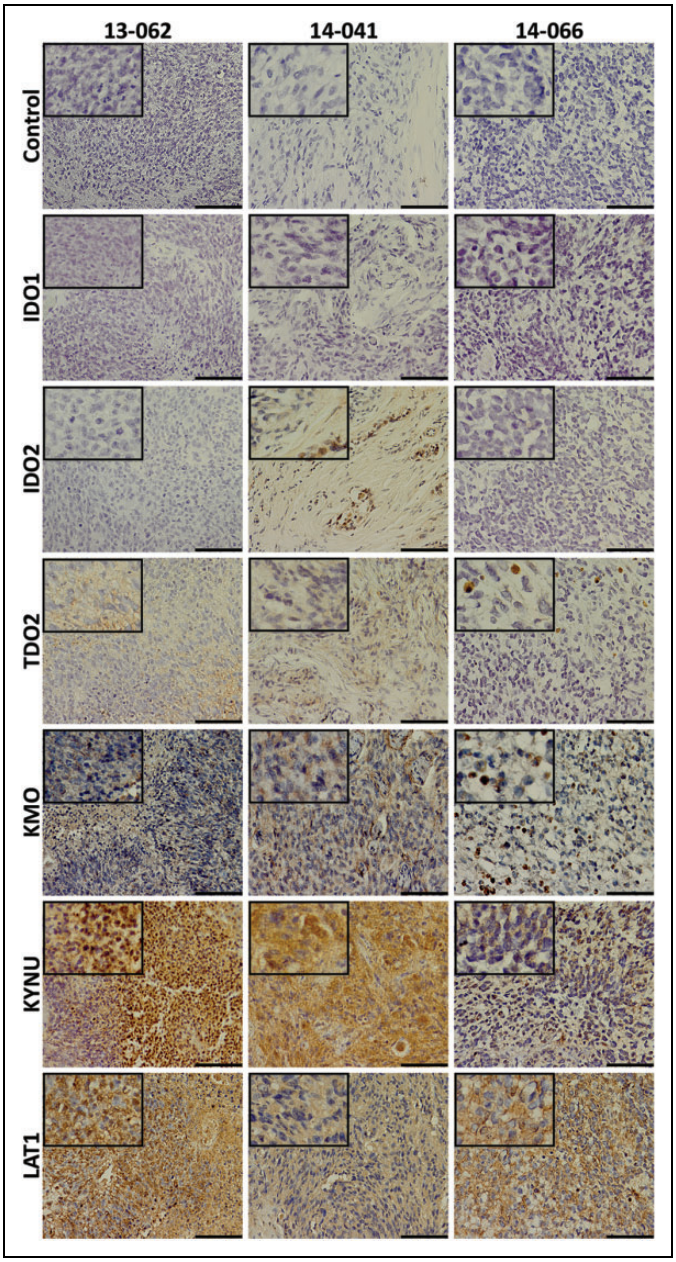

Figure 5. Immunostaining for kynurenine pathway (KP) elements in patient-derived xenograft (PDX) tumor tissue. Immunohistochemical staining of left column: 13-062 PDX tumor tissue; middle column: 14-041 PDX tumor tissue; and right column: 14-066 PDX tumor tissue for secondary antibody only control; the rate-limiting enzymes indoleamine 2,3-dioxygenase (IDO) 1, IDO2, and tryptophan 2,3-dioxygenase (TDO2); downstream enzymes kynureninase (KYNU) and kynurenine 3-monooxygenase (KMO); and L-type amino acid transporter 1 (LAT1). Staining of KP enzymes is weakest in the 14-066 PDX, although a moderate signal for LAT1 is observed. The length of the scale bar is 100 μm. Insets: 4× greater magnification than the larger image.

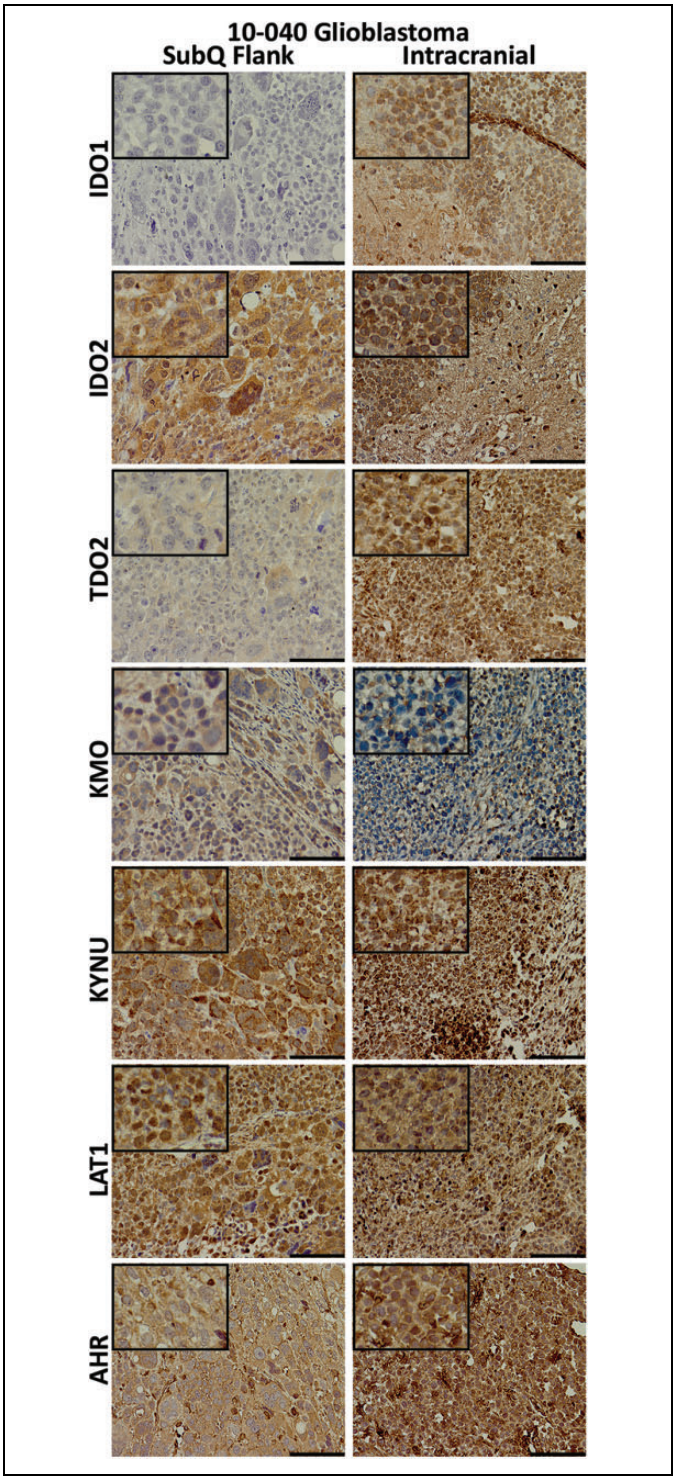

Figure 6. Immunohistochemical staining of the 10-040 patient-derived xenograft (PDX) models. Tissues were collected from the mouse subcutaneous (subQ) flank tumor (left) and the intracranial (right) mouse models. Tissues were stained for the kynurenine pathway (KP) enzymes, L-type amino acid transporter 1 (LAT1), and the transcription factor aryl hydrocarbon receptor (AHR). For all except kynurenine 3-monooxygenase (KMO), staining was equivalent or greater in the intracranial tumor. The length of the scale bar is 100 μm. Insets: 4× greater magnification than the larger image.

analogs such as AMT will be of greater importance. The potential for clinical imaging of the KP in humans with AMT-PET has been extensively studied in brain tumors,

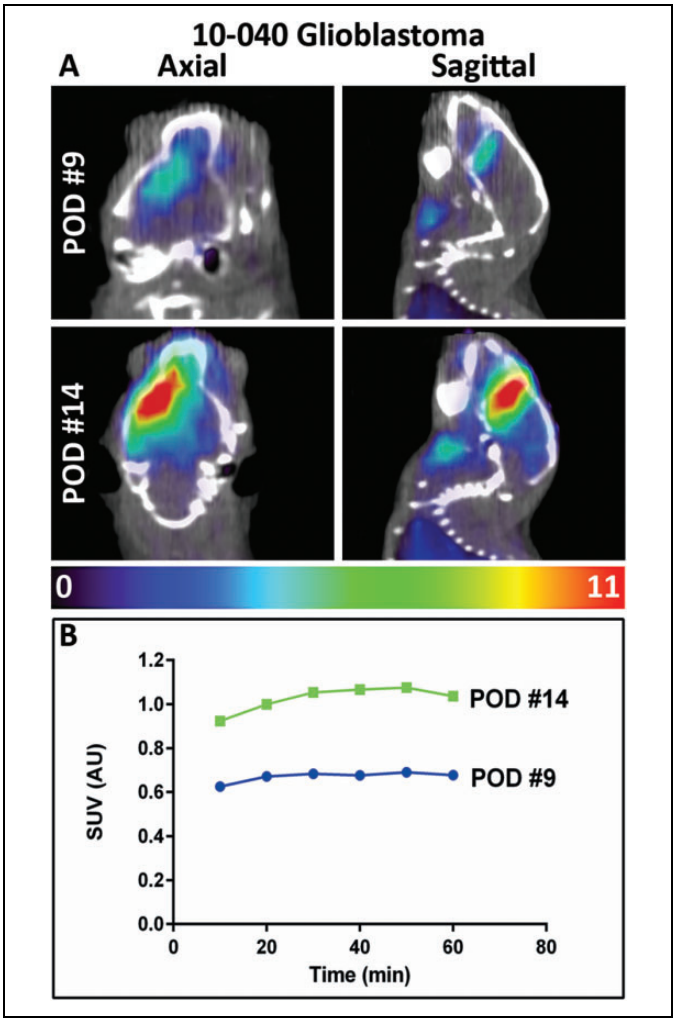

Figure 7. Analysis of orthotopic patient-derived xenograft (PDX) model of 10-040 tumor. A, Axial (left) and sagittal (right) views of α-[^{11}C]-methyl-L-tryptophan (AMT)-positron emission tomography (PET) and coregistered computed tomography (CT) scan for a mouse bearing an intracranial 10-040 PDX tumor. The first scan (post-operative day [POD] #9) shows modest AMT uptake in the injected hemisphere. At the time of the second scan (POD #14), AMT uptake was markedly increased. B, Plot of time versus AMT uptake calculated as standardized uptake values (SUVs). The colored scale bar below the images indicates the range of SUVs.

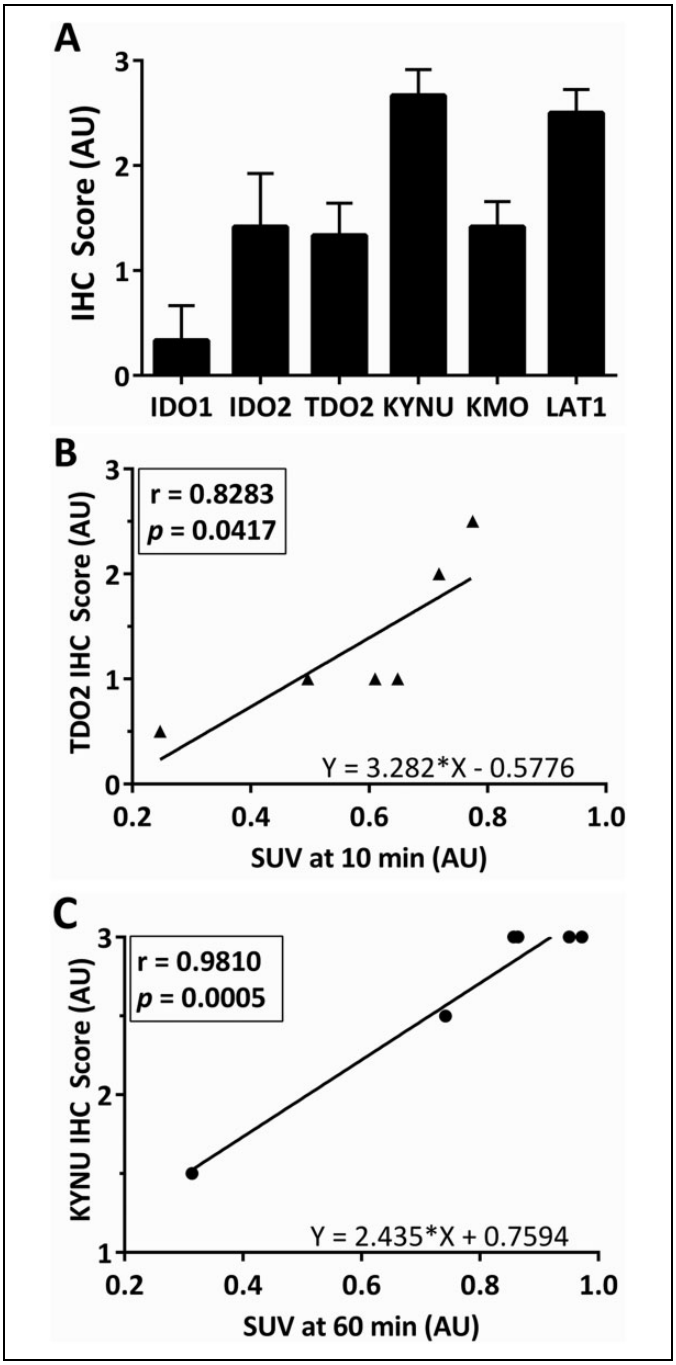

Figure 8. Statistical analyses of immunohistochemical (IHC) scores and α-[^{11}C]-methyl-L-tryptophan (AMT)-positron emission tomography (PET) standardized uptake values (SUVs). A, Staining of the tissue sections from each mouse included in this study was scored as described in the Methods' section. Bars represent mean IHC scores + standard error of the mean (SEM). B, Plot of Pearson correlation for mouse tryptophan 2,3-dioxygenase (TDO2) IHC scores and SUVs at 10 minutes. C, Plot of Pearson correlation for mouse kynureninase (KYNU) IHC scores and SUVs at 60 minutes.

including high-grade gliomas,[23] low-grade gliomas,[21] metastatic brain tumors,[28] and, most recently, meningiomas.[43] To determine the feasibility of using this powerful molecular imaging technique preclinically, we generated PDX models, as they are an authentic embodiment of the heterogeneity observed in human cancers.[44,45] Similar to those studies, our PDX models mimicked the AMT imaging characteristics as well as the correlation of tissue staining of the KP elements as found in our recent human study,[43] again displaying the usefulness of PDX models. This pilot study demonstrates our ability to examine TRP metabolism in vivo in mice bearing human GBM tumors with AMT-PET imaging and provides a highly relevant biological platform for preclinical studies.

Overall, our IHC data confirm KP's prominence in both patient and PDX GBM tissue (Figures 3 and 8A). Although Uyttenhove et al previously reported observing IDO1 staining

in 90% of their GBM tissues,[13] we detected IDO1 in only 2 of 7 tumors (13-058 patient and 10-040 intracranial model). We found that the predominant rate-limiting enzymes are IDO2 and TDO2, which were detected in 5 of 7 and 7 of 7 samples, respectively. This ample TDO2 staining agrees with the findings of Opitz et al, which suggests that TDO2 is the primary rate-limiting enzyme within gliomas.[9] Additionally, our mouse TDO2 staining positively correlates with the SUV for the uptake of the AMT tracer at 10 minutes, further suggesting that TDO2 has a prominent role in initial TRP metabolism in gliomas. Interestingly, tumor 14-066 had minimal AMT uptake and low or no immunostaining for the KP enzymes, although positive staining for the LAT1 transporter. Therefore, we believe the low abundance of rate-limiting enzymes, in conjunction with the low tumor cell density and abnormal tumor architecture, lead to the lack of AMT uptake.

Although we generally found little to no IDO1 expression in most of our tumor tissues, the intracranial xenograft tumor displayed abundant IDO1 immunostaining, even though the corresponding subQ tumor did not. It has been determined in GBM that KYN (and also kynurenic acid) is an endogenous ligand of AHR,[9,46] which has been shown to induce the expression of IDO1 and IDO2,[47] and is part of an autocrine loop leading to constitutive IDO1 expression.[48] Although AHR is present in the subQ mouse tumor, the intensity appears greater in the intracranial tumor, suggesting that this regulatory loop may be active in our model. Our orthotopic model would therefore be suitable to further explore the relationships between the TRP-catabolizing enzymes and the tumor-promoting AHR.

Finally, we demonstrated the ability to measure dynamic changes in TRP metabolism in the intracranial GBM model (Figure 7), with the increase in AMT uptake due to the putative tumor growth in the interval between scans. Additional studies are warranted to confirm this hypothesis. Although limited in scope, our study reinforces the value of PDX models and serves as proof of principle for use of AMT-PET to monitor TRP metabolism in preclinical models. As the field advances in the development of novel therapeutics targeting the enzymes of the KP, our PDX models can be used to test these therapeutics and hopefully improve clinical outcomes for patients with GBM.

Acknowledgments

We would like to thank Xin Lu, MS and Kirk Douglas, BS for performing the micro-PET studies and Kiara P. Brooks for helping with the IHC. We are grateful to the entire staff of the PET Center, Children's Hospital of Michigan, and to our patients for their participation.

Authors' Note

The authors report no conflict of interest or financial disclosure. Dr Mittal and Dr Juhász contributed to the manuscript equally.

Declaration of Conflicting Interests

The author(s) declared no potential conflicts of interest with respect to the research, authorship, and/or publication of this article.

Funding

The author(s) disclose receipt of the following financial support for the research, authorship, and/or publication of this article: The study was supported by a grant (R01 CA123451 to C.J. and S.M.) from the National Cancer Institute; a grant from the Fund for Medical Research and Education, Wayne State University School of Medicine (to S.M.); and a Strategic Research Initiative Grant from the Karmanos Cancer Institute (to S.M. and C.J.). A.R.G. is supported by the Dean's Diversity Fellowship awarded by Wayne State University. The Animal Model and Therapeutics Evaluation Core, the Microscopy, Imaging and Cytometry Resources Core, and the Biobanking and Correlative Sciences Core are supported, in part, by NIH Center Grant P30 CA022453 to the Karmanos Cancer Institute at Wayne State University.

References

1. Ostrom QT, Gittleman H, Liao P, et al. CBTRUS statistical report: primary brain and central nervous system tumors diagnosed in the United States in 2007-2011. *Neuro Oncol*. 2014; 16(suppl 4):iv1-iv63.
2. Xie Q, Mittal S, Berens ME. Targeting adaptive glioblastoma: an overview of proliferation and invasion. *Neuro Oncol*. 2014; 16(suppl 4):1575-1584.
3. Stupp R, Mason WP, van den Bent MJ, et al. Radiotherapy plus concomitant and adjuvant temozolomide for glioblastoma. *N Engl J Med*. 2005;352(10):987-996.
4. Zeng T, Cui D, Gao L. Glioma: an overview of current classifications, characteristics, molecular biology and target therapies. *Front Biosci (Landmark Ed)*. 2015;20:1104-1115.
5. Peters JC. Tryptophan nutrition and metabolism: an overview. *Adv Exp Med Biol*. 1991;294:345-358.
6. Frumento G, Rotondo R, Tonetti M, Damonte G, Benatti U, Ferrara GB. Tryptophan-derived catabolites are responsible for inhibition of T and natural killer cell proliferation induced by indoleamine 2,3-dioxygenase. *J Exp Med*. 2002;196(4): 459-468.
7. Fallarino F, Grohmann U, You S, et al. The combined effects of tryptophan starvation and tryptophan catabolites down-regulate T cell receptor zeta-chain and induce a regulatory phenotype in naive T cells. *J Immunol*. 2006;176(11):6752-6761.
8. Adams S, Teo C, McDonald KL, et al. Involvement of the kynurenine pathway in human glioma pathophysiology. *PLoS One*. 2014;9(11):e112945.
9. Opitz CA, Litzenburger UM, Sahm F, et al. An endogenous tumour-promoting ligand of the human aryl hydrocarbon receptor. *Nature*. 2011;478(7968):197-203.
10. Ott M, Litzenburger UM, Rauschenbach KJ, et al. Suppression of TDO-mediated tryptophan catabolism in glioblastoma cells by a steroid-responsive FKBP52-dependent pathway. *Glia*. 2015; 63(1):78-90.
11. Miyazaki T, Moritake K, Yamada K, et al. Indoleamine 2,3-dioxygenase as a new target for malignant glioma therapy. Laboratory investigation. *J Neurosurg*. 2009;111(2):230-237.
12. Pilotte L, Larrieu P, Stroobant V, et al. Reversal of tumoral immune resistance by inhibition of tryptophan 2,3-dioxygenase. *Proc Natl Acad Sci U S A*. 2012;109(7):2497-2502.

13. Uyttenhove C, Pilotte L, Theate I, et al. Evidence for a tumoral immune resistance mechanism based on tryptophan degradation by indoleamine 2,3-dioxygenase. *Nat Med*. 2003;9(10): 1269-1274.
14. Gramatzki D, Pantazis G, Schittenhelm J, et al. Aryl hydrocarbon receptor inhibition downregulates the TGF-beta/Smad pathway in human glioblastoma cells. *Oncogene*. 2009;28(28):2593-2605.
15. Platten M, Wick W, Van den Eynde BJ. Tryptophan catabolism in cancer: beyond IDO and tryptophan depletion. *Cancer Res*. 2012; 72(21):5435-5440.
16. Diksic M, Nagahiro S, Chaly T, Sourkes TL, Yamamoto YL, Feindel W. Serotonin synthesis rate measured in living dog brain by positron emission tomography. *J Neurochem*. 1991;56(1): 153-162.
17. Diksic M, Nagahiro S, Sourkes TL, Yamamoto YL. A new method to measure brain serotonin synthesis in vivo. I. Theory and basic data for a biological model. *J Cereb Blood Flow Metab*. 1990;10(1):1-12.
18. Diksic M, Tohyama Y, Takada A. Brain net unidirectional uptake of alpha-[14c]methyl-L-tryptophan (alpha-MTrp) and its correlation with regional serotonin synthesis, tryptophan incorporation into proteins, and permeability surface area products of tryptophan and alpha-MTrp. *Neurochem Res*. 2000;25(12):1537-1546.
19. Alkonyi B, Mittal S, Zitron I, et al. Increased tryptophan transport in epileptogenic dysembryoplastic neuroepithelial tumors. *J Neurooncol*. 2012;107(2):365-372.
20. Juhasz C, Chugani DC, Muzik O, et al. In vivo uptake and metabolism of alpha-[^{11}C]methyl-L-tryptophan in human brain tumors. *J Cereb Blood Flow Metab*. 2006;26(3):345-357.
21. Juhasz C, Muzik O, Chugani DC, et al. Differential kinetics of alpha-[^{11}C]methyl-L-tryptophan on PET in low-grade brain tumors. *J Neurooncol*. 2011;102(3):409-415.
22. Juhasz C, Dwivedi S, Kamson DO, et al. Comparison of amino acid positron emission tomographic radiotracers for molecular imaging of primary and metastatic brain tumors. *Mol Imaging*. 2014;13.
23. Kamson DO, Mittal S, Robinette NL, et al. Increased tryptophan uptake on PET has strong independent prognostic value in patients with a previously treated high-grade glioma. *Neuro Oncol*. 2014;16(10):1373-1383.
24. Michelhaugh SK, Guastella AR, Varadarajan K, et al. Development of patient-derived xenograft models from a spontaneously immortal low-grade meningioma cell line, KCI-MENG1. *J Transl Med*. 2015; 13:227.
25. Chakraborty PK, Mangner TJ, Chugani DC, et al. A high-yield and simplified procedure for the synthesis of alpha-[^{11}C]methyl-L-tryptophan. *Nucl Med Biol*. 1996;23(8):1005-1008.
26. Loening AM, Gambhir SS. AMIDE: a free software tool for multimodality medical image analysis. *Mol Imaging*. 2003;2(3): 131-137.
27. Fischer AH, Jacobson KA, Rose J, et al. Hematoxylin and eosin staining of tissue and cell sections. *CSH Protoc*. 2008;2008:pdb. prot4986.
28. Kamson DO, Mittal S, Buth A, et al. Differentiation of glioblastomas from metastatic brain tumors by tryptophan uptake and kinetic analysis: a positron emission tomographic study with magnetic resonance imaging comparison. *Mol Imaging*. 2013; 12(5):327-337.
29. van Baren N, Van den Eynde BJ. Tryptophan-degrading enzymes in tumoral immune resistance. *Front Immunol*. 2015;6:34.
30. NewLink Genetics Corporation. Immunotherapy Combination Study in Advanced Previously Treated Non-Small Cell Lung Cancer. In: ClinicalTrialsgov [Internet] Bethesda (MD): National Library of Medicine (US) 2000 - [accessed April 13, 2016, last updated February 2, 2016]; Web site. http://clinicaltrials.gov/ct2/show/record/NCT02460367. NLM Identifier: NCT02460367.
31. NewLink Genetics Corporation. Study of Chemotherapy in Combination With IDO Inhibitor in Metastatic Breast Cancer. In: ClinicalTrialsgov [Internet] Bethesda (MD): National Library of Medicine (US) 2000 - [accessed April 13, 2016, last updated March 14, 2016]; Web site. http://clinicaltrials.gov/ct2/show/record/NCT01792050. NLM Identifier: NCT01792050.
32. NewLink Genetics Corporation. Study of IDO Inhibitor in Combination With Ipilimumab for Adult Patients With Metastatic Melanoma. In: ClinicalTrialsgov [Internet] Bethesda (MD): National Library of Medicine (US) 2000 - [accessed April 13, 2016, last updated March 22, 2016]; Web site. http://clinicaltrials.gov/ct2/show/record/NCT02073123. NLM Identifier: NCT02073123.
33. NewLink Genetics Corporation. Study of IDO Inhibitor in Combination With Gemcitabine and Nab-Paclitaxel in Patients With Metastatic Pancreatic Cancer. In: ClinicalTrialsgov [Internet] Bethesda (MD): National Library of Medicine (US) 2000 - [accessed April 13, 2016, last updated February 2, 2016]; Web site. http://clinicaltrials.gov/ct2/show/record/NCT02077881. NLM Identifier: NCT02077881.
34. Rosewell Park Cancer Institute. DEC-205/NY-ESO-1 Fusion Protein CDX-1401, Poly ICLC, and IDO1 Inhibitor INCB024360 in Treating Patients With Ovarian, Fallopian Tube, or Primary Peritoneal Cancer in Remission. In: ClinicalTrialsgov [Internet] Bethesda (MD): National Library of Medicine (US) 2000 - [accessed April 13, 2016, last updated March 22, 2016]; Web site. http://clinicaltrials.gov/ct2/show/record/NCT02166905. NLM Identifier: NCT02166905.
35. Rosewell Park Cancer Institute. Vaccine Therapy and IDO1 Inhibitor INCB024360 in Treating Patients With Epithelial Ovarian, Fallopian Tube, or Primary Peritoneal Cancer Who Are in Remission. In: ClinicalTrialsgov [Internet] Bethesda (MD): National Library of Medicine (US) 2000 - [accessed April 13, 2016, last updated December 17, 2013]; Web site. http://clinicaltrials.gov/ct2/show/record/NCT01982487. NLM Identifier: NCT01982487.
36. Incyte Corporation. A Phase 2 Study of the IDO Inhibitor INCB024360 Versus Tamoxifen for Subjects with Biochemical-recurrent-only EOC, PPC or FTC Following Complete Remission With First-line Chemotherapy. In: ClinicalTrialsgov [Internet] Bethesda (MD): National Library of Medicine (US) 2000 - [accessed April 13, 2016, last updated November 4, 2015]; Web site. http://clinicaltrials.gov/ct2/show/record/NCT01685255. NLM Identifier: NCT01685255.
37. Incyte Corporation. A Phase 1/2 Randomized, Blinded, Placebo Controlled Study of Ipilimumab in Combination With INCB024360 or Placebo in Subjects With Unresectable of

Metastatic Melanoma. In: ClinicalTrialsgov [Internet] Bethesda (MD): National Library of Medicine (US) 2000 - [accessed April 13, 2016, last updated April 1, 2016]; Web site. http://clinicaltrials.gov/ct2/show/record/NCT01604889. NLM Identifier: NCT01604889.

38. Fred Hutchinson Cancer Research Center. INCB024360 and Vaccine Therapy in Treating Patients With Stage III-IV Melanoma. In: ClinicalTrialsgov [Internet] Bethesda (MD): National Library of Medicine (US) 2000 - [accessed April 13, 2016, last updated March 11, 2016]; Available from: http://clinicaltrials.gov/ct2/show/record/NCT01961115. NLM Identifier: NCT01961115.
39. NewLink Genetics Corporation. Study of IDO Inhibitor and Temozolomide for Adult Patients With Primary Malignant Brain Tumors. In: ClinicalTrialsgov [Internet] Bethesda (MD): National Library of Medicine (US) 2000 - [accessed April 13, 2016, last updated March 25, 2016]; Web site. http://clinicaltrials.gov/ct2/show/record/NCT02052648. NLM Identifier: NCT02050648.
40. Main Line Health. IDO2 Genetic Status Informs the Neoadjuvant Efficacy of Chloroquine (CQ) in Brain Metastasis Radiotherapy. In: ClinicalTrialsgov [Internet] Bethesda (MD): National Library of Medicine (US) 2000 - [accessed April 13, 2016, last updated April 7, 2015]; Web site. http://clinicaltrials.gov/ct2/show/record/NCT01727531. NLM Identifier: NCT01727531.
41. Eldredge HB, Denittis A, Duhadaway JB, et al. Concurrent whole brain radiotherapy and short-course chloroquine in patients with brain metastases: a pilot trial. *J Radiat Oncol*. 2013;2(3).
42. Sotelo J, Briceno E, Lopez-Gonzalez MA. Adding chloroquine to conventional treatment for glioblastoma multiforme: a randomized, double-blind, placebo-controlled trial. *Ann Intern Med*. 2006;144(5):337-343.
43. Bosnyák E, Kamson DO, Guastella AR, et al. Molecular imaging correlates of tryptophan metabolism via the kynurenine pathway in human meningiomas. *Neuro Oncol*. 2015;17(9):1284-1292.
44. Gandara DR, Lara PN Jr, Mack PC. Patient-derived xenografts for investigation of acquired resistance in oncogene-driven cancers: building a better mousetrap. *J Clin Oncol*. 2015;33(26):2839-2840.
45. Siolas D, Hannon GJ. Patient-derived tumor xenografts: transforming clinical samples into mouse models. *Cancer Res*. 2013;73(17):5315-5319.
46. DiNatale BC, Murray IA, Schroeder JC, et al. Kynurenic acid is a potent endogenous aryl hydrocarbon receptor ligand that synergistically induces interleukin-6 in the presence of inflammatory signaling. *Toxicol Sci*. 2010;115(1):89-97.
47. Vogel CF, Goth SR, Dong B, et al. Aryl hydrocarbon receptor signaling mediates expression of indoleamine 2,3-dioxygenase. *Biochem Biophys Res Commun*. 2008;375(3):331-335.
48. Litzenburger UM, Opitz CA, Sahm F, et al. Constitutive IDO expression in human cancer is sustained by an autocrine signaling loop involving IL-6, STAT3 and the AHR. *Oncotarget*. 2014;5(4):1038-1051.